Plasma synthesis

DOI: 10.1002/smll.200800278

Spontaneous Growth of Superstructure α-Fe_2O_3 Nanowire and Nanobelt Arrays in Reactive Oxygen Plasma**

Uroš Cvelbar, Zhiqiang Chen, Mahendra K. Sunkara, and Miran Mozetič*

One-dimensional α-Fe_2O_3 is a promising nanomaterial for advanced applications in catalysis and water splitting, environmental protection, sensors, dye solar cells, magnetic storage media, bioprocessing, and controlled drug delivery and detection, especially as carriers of antigens for prion detection and PCR manipulation.[1] α-Fe_2O_3 nanowires have been successfully synthesized by various methods based on templates,[2] hydrothermal conditions,[3] sol–gel-mediated reactions,[4] solvothermal conditions,[5] gas decomposition,[6] direct thermal oxidation (in a gas atmosphere of CO_2, SO_2, O_2, and NO_2),[7] chemical vapor deposition (CVD),[8] and plasma-enhanced chemical vapor deposition (PECVD).[9] The methods based on direct thermal oxidation, gas decomposition, and CVD reported to date require long synthesis times and high temperatures and therefore limit the efficiency of oxide nanowire synthesis.[6–9] The application and commercialization of nanowires or nanobelts requires simple synthetic methods that can be scaled for both large areas and large quantities.

Recently, we discovered a new universal method for the synthesis of transition metal oxide nanowires and nanobelts by direct plasma oxidation of bulk materials. It has been successfully applied for the rapid synthesis of high-density niobium oxide nanowires.[10] In this process, there is no continuous supply of metallic species from the vapor phase, and thus the nanowires are not expected to grow in a tip-led fashion. Several questions regarding the nucleation and growth mechanisms for nanowire growth during plasma oxidation of solid foils are yet to be answered. Specifically, the role of the substrate temperature during plasma oxidation, the independent control of nucleation and growth, and the rational choice of parameters for growing nanowires of other materials by this method are not clear. To gain more insight, we chose to investigate the large-scale synthesis of α-Fe_2O_3 (hematite) by using solid-phase iron material, because the Fe–O phase diagram is more readily available. Primarily, we conducted a systematic investigation of the experimental conditions to understand both nucleation and growth mechanisms that are responsible for promoting the growth of nanowires and nanobelts in our plasma oxidation scheme. The findings presented herein could be used further to help design the plasma oxidation scheme for synthesizing other metal oxide nanowire systems.

In a typical plasma oxidation procedure, we used commercial iron sheets that were continuously exposed to oxygen glow discharge with an O-atom density of approximately 2×10^{21} m^{-3} and ion density of $1–6 \times 10^{-16}$ m^{-3} for 2 min. Such plasma exposure resulted in vertical arrays of iron oxide nanowires (NW) on a large area of the iron sheet as shown in Figure 1a. The nanowires typically grew perpendicular to the surface. Small deviations from vertical growth were also observed. Such nonvertical growth could be due to a number of factors such as parallel orientation of the sample surface to the gas flow, surface roughness, and plasma gas turbulence in the reactor caused by oxygen gas leaking into or pumping out of the vacuum system. The nanowire diameter distribution on a 100-μm^2 sample area from Figure 1a is presented in Figure 1c. The average nanowire is 120 nm wide at the base, but becomes narrower and sharpens towards the tip. From the distribution of the nanowire diameters, we can conclude that spontaneous nucleation takes place. If the plasma parameters (e.g. atom or ion flux) change, then the resulting growth leads either to nanobelt growth (Figure 1b) or to the lack of any 1D nanostructure growth.

The Raman spectrum presented in Figure 2 clearly shows an α-Fe_2O_3 phase for the synthesized nanowires and nanobelts. The peak positions are in good agreement with previously reported results.[1b,7a] This further confirms the contention that the nanowires are trigonal Fe_2O_3. There is a small variation between the Raman peak positions for the nanowires and the bulk state in the region 400–700 cm^{-1}. The shifting of Raman peaks to higher values means blue shifting of Raman peaks (higher wavenumbers mean lower wavelengths).

To understand the formation process of the iron oxide nanostructures, we carried out plasma-parameter-dependent experiments and monitored the surface temperature, during which samples were collected at the end of 2-min plasma treatment. The surface reactions of reactive oxygen plasma radicals, mainly by recombination of neutral O atoms and oxygen (O^+, O^-) ions with iron material, heats up the surface. The heating is strongly dependent on the density of the atoms or ions inside the plasma-discharge vessel. The probability for

[*] Prof. U. Cvelbar, Prof. M. Mozetič
Jožef Stefan Institute
Jamova cesta 39
Ljubljana, SI-1000 (Slovenia)
E-mail: uros.cvelbar@ijs.si
Prof. M. Sunkara
Chemical Engineering Department and
Institute for Advanced Materials & Renewable Energy
University of Louisville
Louisville KY, 40292 (USA)
E-mail: mahendra@louisville.edu
Dr. Z. Chen
Institute for Advanced Materials & Renewable Energy
University of Louisville
Louisville KY, 40292 (USA)

[**] The authors acknowledge the support of the US Department of Energy for the Institute of Advanced Materials and Renewable Energy at the University of Louisville (DE-FG02-05ER64071), the US-DOE through DOE-EPSCoR Program (DE-FG02-07ER46375), and the support of Sloverian Ministry for Science and Technology (BI-SLO-ZDA-2006/07-01).

Supporting Information is available on the WWW under http://www.small-journal.com or from the author.

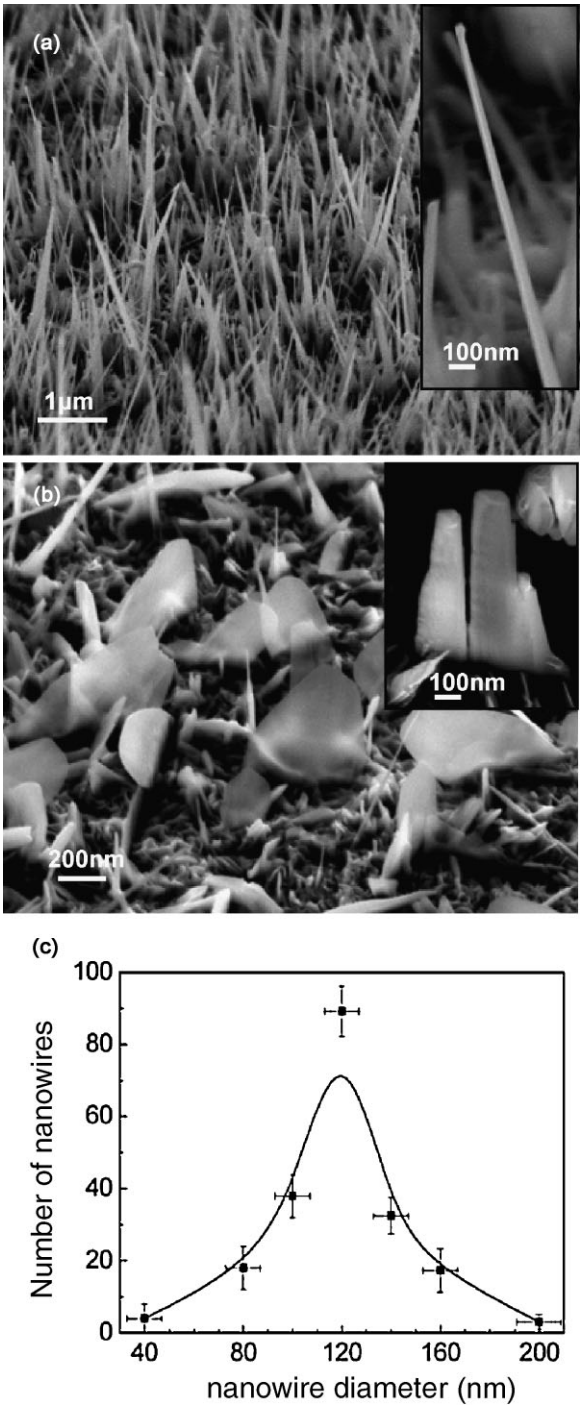

Figure 1. SEM images of iron oxide nanostructures grown on Fe bulk material during oxygen plasma treatment at 100 Pa. The entire surface is covered with a large array of α-Fe_2O_3 a) nanowires or b) nanobelts. The average diameter of the nanowires is 120 nm. c) The distribution curve of nanowire diameter (a) within a 100-μm^2 area indicates spontaneous nucleation of nanowires.

surface recombination and loss of neutral oxygen atom energy (2.5 eV) is approximately 0.4 for iron, but the probability of recombination and consequential loss of ion energy (3–10 eV) is almost 1.[11] Therefore, the ions can recombine on the surface at 2.5-fold higher probability than atoms, and they can generate up to threefold more energy that is converted into

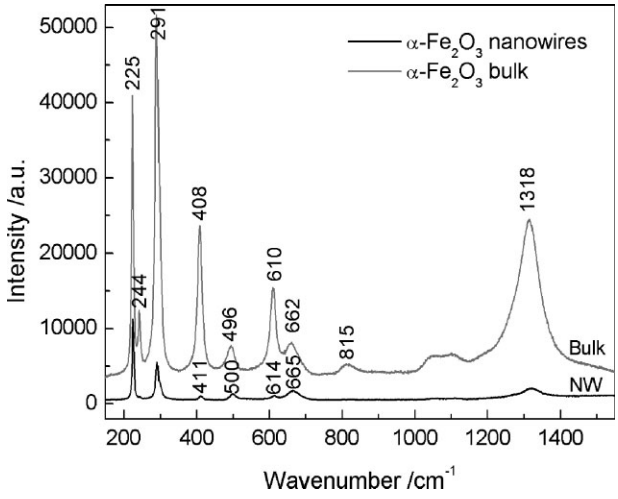

Figure 2. Raman spectroscopy reveals the α-Fe_2O_3 oxide layer, nanowires, and nanobelts on bulk Fe surface prepared by oxygen plasma treatment.

thermal heating of the substrate. The variability of atom/ion density and the energy of the ions can be used to manipulate the flux of reactive plasma radicals to the surface and for heating of the surface. The above variations were done under a range of plasma parameters in which the growth of nanostructures is possible. As radical recombination can influence nanowire growth, the temperature of the upper surface layer was monitored. The density of neutral O atoms at the reactor wall was approximately constant at 2×10^{21} m^{-3}. The ion density and energy was changed to study the influence of plasma parameters on nanowire growth.

The changes in the temperature of the samples during nanostructure synthesis by plasma oxidation are shown in Figure 3. After the oxygen plasma is initiated, the temperatures of all samples exposed to the glow plasma discharge increase rapidly as a result of the exothermic oxidation

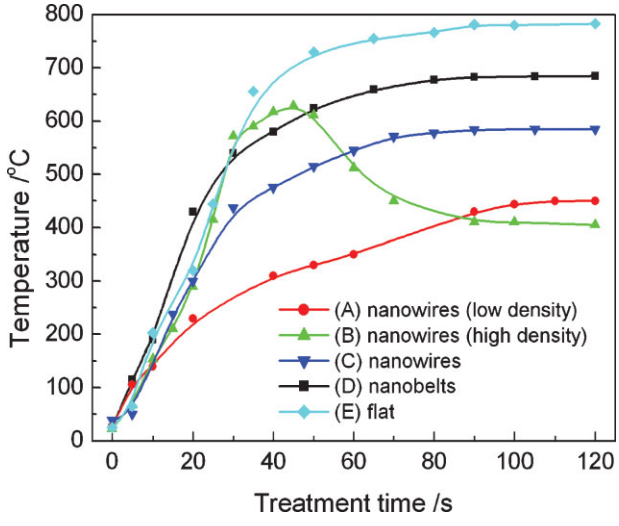

Figure 3. The surface temperature of the iron oxide samples during plasma treatment and synthesis of nanowires, nanobelts, or flat thin films.

reaction, the creation of an oxide layer, and the reactive radical surface recombination. If there are too many higher-energy ions in the plasma, then the heating is too fierce and no nanostructures are created on the surface. This holds true when the surface temperature increases up to 780 °C, and only a flat oxide layer is created. When the density of O atoms is the same, a plasma that contains energy-poorer ions leads to the formation of nanobelts. This occurs when the surface temperature rises to 680 °C. At lower temperatures of the iron surface, nanowires grow preferentially to nanobelts. When the surface temperature during synthesis is even lower than 570 °C, then the density of the nanowires is lower, and their average diameter also decreases (see Figure 1c). Most importantly, the initial temperature jump or so-called plasma overheating before the surface temperature reaches equilibrium determines the density of the nanowires (presented as curve B of high-density nanowires in Figure 3 and corresponds to Figure 1a and 1c). This means that the initial temperature jump influences the nucleation density of the resulting nanowires. This can also be seen from the data in Table 1. As seen in Figure 3, curve A, the density of the synthesized nanowires is lower with a low initial temperature rise. The resulting nanowires are short (≈100 nm) and have smaller diameters (≈10 nm). The nanowire density is higher when the initial temperature rise is higher and similar for both surfaces under constant radical flux without initial surface overheating. The explanation for this can be found in the phase diagram of Fe–O transitions.[12] The phase transition of iron with soluble oxygen to the Fe_3O_4 phase or to the α-Fe_2O_3 phase takes place at 570 °C and 580 °C, respectively. As it is difficult to target the Fe_3O_4 phase temperature for nucleation, α-Fe_2O_3 nuclei are normally formed. The size and density of the nuclei are determined by the plasma parameters that control the surface temperature and the oxygen solubility in iron.

The nucleation and growth stages of the synthesized nanowires could be better understood through the following, detailed structural characterization. The resulting single-crystal α-Fe_2O_3 nanostructures grow along the [110] directions. The typical structural characteristics of a single nanowire synthesized by using the plasma oxidation technique is illustrated in Figure 4. The α-Fe_2O_3 nanowires are 165 nm in diameter and gradually decrease towards the end in an ≈1-μm-long nanowire (Figure 4a). The tip, the neck, and the matured body can be clearly seen in Figures 4b and 4c. The HREM (high-resolution electron microscopy) images and the corresponding FFT (fast Fourier transform) patterns show that there is an oxygen-vacancy ordering in the nanowires (Figure 4c). The corresponding FFT images clearly showed that there are no extra maxima in the neck region, but there are extra maxima in the matured nanowire and the NW tip. Furthermore, the ordering bands are clearly shown in the HREM image taken from the tip (Figure 4b). The FFT images illustrate a superlattice structure with ordering of the oxygen-vacancy planes. The details of our analysis of the FFT patterns and the corresponding long-range ordering of the oxygen-vacancy planes are discussed in detail elsewhere.[13] The analysis of Figure 4 indicates that the extra maxima originated from oxygen-vacancy ordering on every fourth plane of (1–12) in α-Fe_2O_3. Additional long-range ordering of oxygen vacancies was also found on every 10th (3–30) plane with the same ordering distance of 1.45 nm. This implies that the same oxygen-vacancy ordering occurs throughout the whole wire, even after merger at the base occurs. Note that the observed ordering plane (1–12) or (3–30) is linear to the direction of growth of the nanowire. Also, two equal d spacings, 0.25 nm, from the mature body are consistent with those from the nanowire base. So far, the structure of the entire α-Fe_2O_3 wire is clear: ordered α-Fe_2O_3 with vacancy plane through the mature nanowire and tip, but blocked at the neck region containing stochiometric Fe_2O_3.

The same ordering as that in the nanowires is also found within the nanobelt structures (see Supporting Information). They share the same ordering plane (3–30), which is also parallel to the growth direction. This implies that the nanobelts and nanowires show the same long-range ordering of oxygen vacancies with a d spacing of about 1.45 nm. The superstructures in α-Fe_2O_3 are similar to the superlattice structures in Cr_2O_3 nanobelts and nanorods, but the two ordering distances 0.74 and 1.64 nm found are different.[14]

The TEM analysis clearly indicates that the nanowires have a characteristic tip from the nucleation stage. Like in all α-Fe_2O_3 synthesized nanostructures, the tip and the body follow the same oxygen deficiency in every tenth (3–30) plane. However, the neck region has no ordering features and seems to represent the non-steady-state portion of the initial stages of the growth process immediately after the spontaneous nucleation stage. The narrowing of a nanowire towards the tip further indicates basal growth. High ion densities and energies could promote later growth of nanowires and merge them to become nanobelts. The intermediate stage between the two phases is seen in the form of palm-shaped nanobelts in which nanowires are merged to form the belt (inset in Figure 1b). The nanobelts occur at higher temperatures, which could be explained with higher surface diffusion of iron atoms on the nanowire surfaces. Although, the nanobelts can be created from intergrowth between adjacent wires, they can also be created from single nanowires or from widening of nanowires at the base (Figure 1 and Table 1). Notably, all

Table 1. Growth dynamics represented with an average number of aligned nanowires and their average basal diameter in different thermal regimes seen in Figure 3.

Sample	Surface Temperature [°C]	Nanowire Density [100 μm^{-2}]	Average Nanowire Diameter [nm]
A	450	70	8 ± 2
B	630–405	194	120 ± 10
C	585	162	110 ± 10
D	685	159	235 ± 40
E	783	0	0

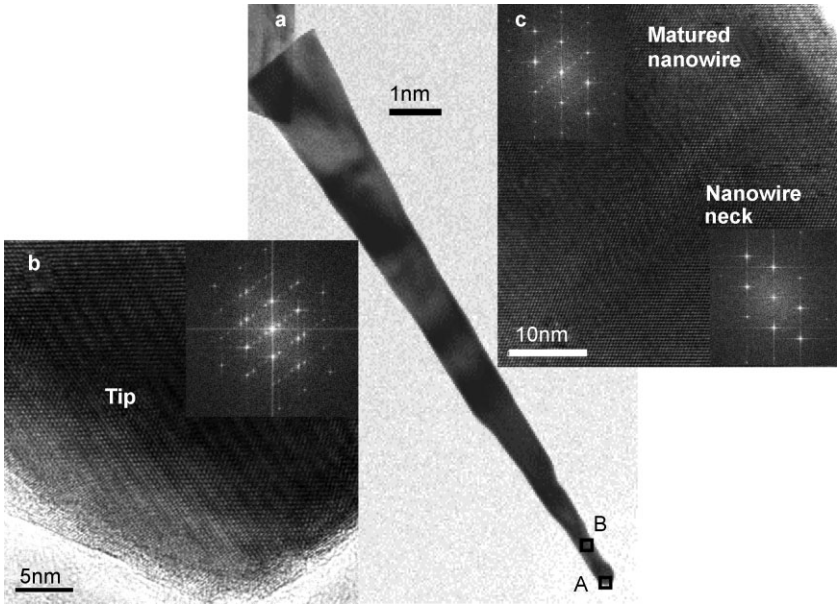

Figure 4. a) High-magnification TEM images of nanowires with HREM image and its FFT image showing oxygen-vacancy ordering in $\alpha - Fe_2O_3 \frac{1}{4}(\bar{1}\ 12)$ plane of b) the nanowire tip and c) the matured nanowire, but not on the nanowire neck area.

nanowires or nanobelts grow in the same manner, irrespective of the type of Fe substrate, for example, Fe clusters or the 2–10-μm Fe_3O_4 layer covering the Fe samples. This shows that the nanostructure morphology is controlled only by plasma parameters and not by the initial Fe substrate layer.

Finally, on the basis of the above observations, the nucleation and growth of metal oxide nanowires is schematically illustrated in Figure 5. During exposure of the Fe clusters or the iron-oxides to oxygen plasma glow, nucleation occurs over a large area of the treated surface. The nucleation occurs spontaneously everywhere on the plasma-treated substrate. However, further growth of the nuclei differs, depending on the substrate temperature. At low temperatures, the growth of the nuclei takes place primarily at the base, leading to nanowire growth, that is, oxidation of the interface between the metal oxide nuclei and the metal substrate. At higher temperatures, the growth of the nuclei can occur in any direction with increased availability of iron atoms and will lead to thin oxide films. First, the nucleation is primarily influenced by the initial surface jump beyond 580 °C, the temperature required for Fe–O phase transition. However, nucleation occurs even when the average measured surface temperature is below the required temperature (e.g. 450 °C), as the exposed parts can be heated to temperatures beyond the Fe–O phase-transition temperature by radical recombination. In such cases, smaller nuclei and density distribution is created. Second, one-dimensional nanostructure growth occurs only when the surface temperature does not exceed 780 °C. When the surface temperature exceeds 780 °C, no nanostructure growth occurs, and only a thin film is formed. When the substrate is cooled below the phase-transition temperature after the nucleation step, the growth of existing nuclei occurs only at the interface owing to the low mobility of the iron atoms at these temperatures. The initial stages of the growth processes can be further understood with the observation of a neck region, that is, complete oxidation with no oxygen-vacancy planes. The HRTEM analysis further proves that the nanowire phase continues with the same phase as nuclei, where the growth is epitaxial from the iron–plasma interface region, as seen from narrowing wires. As the recombination of O atoms on the nanowires is approximately 0.3 and the distance between wires is about 0.5 μm, atoms with a mean free path of 0.17 mm easily reach the interface and are trapped on the surface.[15] Therefore, the diffusion of O atoms along the nanowire can be generally neglected. If the sample temperature is continuously increased to around 600 °C, then nanobelts or palm-shaped nanobelts are created. This is due to the increased mobility of Fe atoms and further growth of

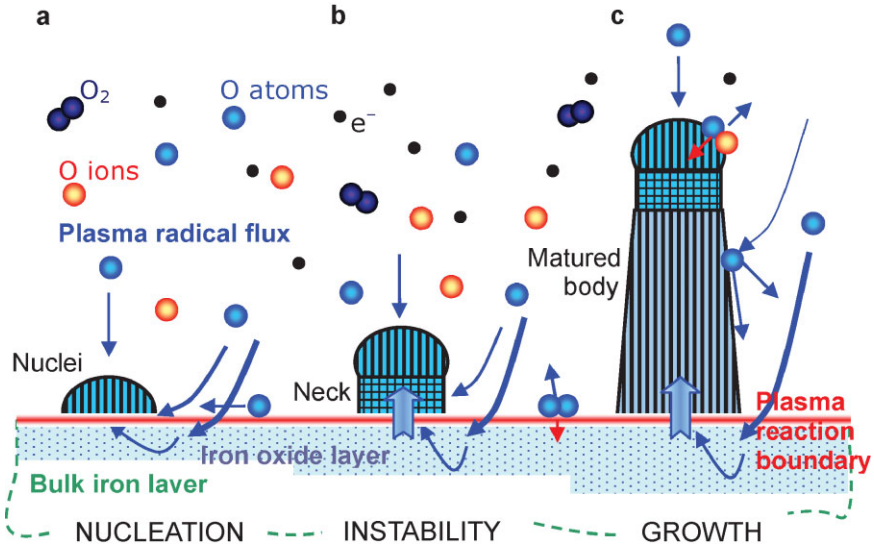

Figure 5. Schematic illustration of the growth mechanism of the metal oxide nanowires from bulk material when exposed to highly dissociated oxygen plasma. Three main stages of nanowire growth are represented: a) nucleation, b) instability, c) growth.

nanowires in another direction to become belts. The nanostructures can be theoretically grown until oxygen atoms are supplied to the surface. The resulting nanowires are thinner when the surface temperature is lower (after the nucleation step) or when the neutral atom flux is constant and the ion flux approaches zero. However, the interface is always disturbed by plasma shutdown, and it is very difficult to assess how much the shutdown influences the creation of the oxide interface layer on the substrate after the plasma synthesis.

As the plasma oxidation described herein is rapid (few seconds), the iron oxide nanowires/nanobelts could be grown both over large areas and in large quantities. Most importantly, the nucleation and growth processes for nanowires with plasma oxidation of solid foils are rationalized. The conceptual understanding of the nucleation and growth stages will help in designing plasma oxidation processes for other metal oxide nanowire systems.

Experimental Section

The nanowires and nanobelts were synthesized directly from the bulk material during exposure of an iron band to oxygen plasmas. A commercially available low-purity (98.85% Fe) iron sheet of thickness 1.7 mm was cut to rectangular pieces of approximately 15×15 mm^2 and exposed to inductively coupled oxygen glow plasma created in a high-frequency discharge.

The experiments were performed in a vacuum system pumped with a two-stage rotary pump with an ultimate pressure of about 0.1 Pa. After the chamber was evacuated to base pressure, commercially available oxygen was continuously leaked into the system. The reactor chamber was maintained at a pressure of 100 Pa during the experiments. The plasma was created by a 27.12 MHz RF generator with a maximum power of 5 kW. The temperature of the sample surface was measured through an IR-transparent window with a Raytec infrared (IR) camera Raynger MX. Plasma characteristics were controlled by using Langmuir and catalytic probes at the reactor wall. The plasma parameters were as follows: electron energy: 3–10 eV, ion density: $1–6 \times 10^{16}$ m^{-3}, neutral oxygen density: $1.6–2.3 \times 10^{21}$ m^{-3}. The samples were exposed to plasma for 120 s.

After the plasma treatment, the samples were analyzed by means of SEM, TEM, selected area diffraction, and Raman spectroscopy. The Synthesized nanowires or nanobelts were scratched from the sample surface, suspended in ethanol, and dispersed on a 300-mesh copper grid with a thin-layer carbon film for TEM observation. The individual nanowires or nanobelts were separated during TEM specimen preparation. High-resolution electron microscopy was carried out with a field-emission gun TECNAI F20 XTWIN TEM equipped with a Gatan GIF 2002 system operated at 200 kV.

Keywords:

iron oxide · nanobelts · nanowires · oxygen plasma

[1] a) S. P. Leary, C. Y. Liu, M. L. J. Apuzzo, *Neurosurgery* **2006**, *58*, 805–823; b) I. Chourpa, L. Douziech-Eyrolles, L. Ngaboni-Okassa, J. F. Fouquenet, S. Cohan-Jonathan, M. Souce, H. Marchais, P. Dubois, *Analyst* **2005**, *130*, 1395–1403; c) K. Ostrikov, *Rev. Mod. Phys.* **2005**, *77*, 489–511; d) H. Tan, *Environ. Sci. Technol.* **2006**, *40*, 5490–5495; e) J. Chen, L. Xu, W. Li, X. Gou, *Adv. Mater.* **2005**, *17*, 582–585; f) Y. Chen, Y.-C. Lee, Y.-L. Chueh, C.-H. Hsieh, M.-T. Chang, L. J. Chou, Z. L. Wang, Y. W. Lan, C. D. Chen, H. Kurata, S. Isoda, *Small* **2007**, *3*, 1356–1361.

[2] a) Y. Peng, H. L. Zhang, S. L. Pan, H. L. Li, *J. Appl. Phys.* **2000**, *87*, 7405–7408; b) L. Y. Zhang, D. S. Xue, X. F. Xu, A. B. Gui, C. X. Gao, *J. Phys.: Condens. Mater.* **2004**, *16*, 4541–4548.

[3] a) D. Chen, L. Gao, *Chem. Phys. Lett.* **2004**, *395*, 316–320; b) M. Pregelj, P. Umek, B. Drolc, B. Jančar, Z. Jagličič, R. Dominko, D. Arčon, *J. Mater. Res.* **2006**, *21*, 2955–2962.

[4] a) H. Wang, X. Zhang, B. Liu, H. Zhao, Y. Li, Y. Huang, *Z. Du, Chem. Lett.* **2005**, *34*, 184–185; b) K. Woo, H. J. Lee, J. P. Ahn, Y. S. Park, *Adv. Mater.* **2003**, *15*, 1761–1764; c) L. S. Zhong, J. S. Hu, H. P. Liang, A. N. Cao, W. G. Song, L. J. Wan, *Adv. Mater.* **2006**, *18*, 2426–2431.

[5] J. Jin, S. Ohkoshi, K. Hashimoto, *Adv. Mater.* **2004**, *16*, 48–51.

[6] a) J. B. Yang, H. Xu, S. X. You, Y. D. Zhou, C. S. Wang, W. B. Yelon, W. J. James, *J. Appl. Phys.* **2006**, *99*, 08Q507; b) J. J. Wu, Y. L. Lee, H. H. Chiang, D. K. P. Wong, *J. Phys. Chem. B: Lett.* **2006**, *110*, 18108–18111.

[7] a) Y. Y. Fu, R. M. Wang, J. Xu, J. Chen, Y. Yan, A. V. Narlikar, H. Zhang, *Chem. Phys. Lett.* **2003**, *379*, 373–379; b) R. Wang, Y. Chen, Y. Fu, H. Zhang, C. Kisielowski, *J. Phys. Chem. B* **2005**, *109*, 12245–12249; c) C. H. Kim, H. J. Chun, D. S. Kim, S. Y. Kim, J. Park, J. Y. Moon, G. Lee, J. Yoon, Y. Jo, M. H. Jung, S. Jung, C. J. Lee, *App. Phys. Lett.* **2006**, *89*, 223103; d) Q. Han, Y. Y. Xu, Y. Y. Fu, H. Zhang, R. M. Wang, T. M. Wang, Z. Y. Chen, *Chem. Phys. Lett.* **2006**, *431*, 100–103.

[8] Y. L. Chueh, M. W. Lai, J. Q. Liang, L. J. Chou, Z. L. Wang, *Adv. Funct. Mater.* **2006**, *16*, 2243–2251.

[9] F. Liu, P. Cao, H. Zhang, J. Tian, C. Xiao, C. Shen, J. Li, H. Gao, *Adv. Mater.* **2005**, *17*, 1893–1897.

[10] M. Mozetič, U. Cvelbar, M. K. Sunkara, S. Vaddiraju, *Adv. Mater.* **2005**, *17*, 2138–2142.

[11] M. Mozetič, A. Vesel, U. Cvelbar, A. Ricard, *Plasma Chem. Plasma Process.* **2006**, *26*, 103–117.

[12] MIT Database [http://noise-complaint.mit.edu/Useful/Science%20&%20Engineering/Binary%20Phase%20Diagrams/Fe%20-%20Iron/], October **2007**.

[13] Z. Chen, U. Cvelbar, M. Mozetič, M. Sunkara, *Chem. Mater.* **2008**, *20*, 3224–3228.

[14] W. Q. Han, L. Wu, A. Stein, Y. Zhu, J. Misewich, J. Warren, *Angew. Chem. Int. Ed.* **2006**, *45*, 6554–6558.

[15] U. Cvelbar, M. Mozetič, *J. Phys. D* **2007**, *40*, 2300–2303.

Received: February 25, 2008
Published online: September 3, 2008

